Numerical simulation and experiment of optothermal response of biological tissue irradiated by continuous xenon lamp

Meizhen Huang (黄梅珍)* and Yaxing Tong (童雅星)

Institute of Optical Engineering, Department of Physics, Shanghai Jiao Tong University, Shanghai 200240, China

**Corresponding author: mzhuang@sjtu.edu.cn*

Received March 28, 2011; accepted May 13, 2011; posted online September 2, 2011

A finite element method computation model for analyzing optothermal interaction of polychromatic light and biology tissue is proposed and proven by experiment. A continuous xenon lamp is employed as an example. First, the spectral energy distribution of the xenon lamp is measured and found to be equivalent to a series of quasi-chromatic light with different central wavelengths, different energies, and certain bandwidth. Next, according to the reported thermal and optical parameters of porcine skin and porcine liver, the temporal temperature distributions of these tissues irradiated by each quasi-chromatic light are simulated. Then, the thermal effect is superimposed to obtain the whole optothermal temporal temperature distribution. Moreover, the optothermal response experiments of fresh porcine skin and porcine liver tissues irradiated by continuous xenon lamp are carried out. The results of the simulation and experiment are analyzed and compared, and are found to be commendably matched.

OCIS codes: 170.1020, 170.3660.

doi: 10.3788/COL201210.011701.

The interaction between light and biological tissue plays a key issue in biomedical optics. A variety of work has been reported on the applications of lasers for clinical research and treatment. These lasers include the CO_2 laser with a wavelength of 10.6 μm, pulsed dye laser with a wavelength of 585 nm, Q-switch infrared laser with a wavelength of 1 064 nm, and Er:YAG laser with a wavelength of 2 940 nm. Bitter Sr. introduced the intense pulsed light (IPL) machines for dermatological therapy. IPL is a noncoherent polychromatic light of high intensity and broad spectrum produced by high-power flash xenon lamp and bandpass filters. A broad spectrum of polychromatic light had been applied to the biomedical-optical research since the photorejuvenation technique was reported[1,2]. The photorejuvenation technique is actually an extension of the traditional laser cosmetic surgery. It is based on the irradiation of the continuous xenon lamp. Its mechanism dates back to the selective effect of photorejuvenation proposed by Anderson *et al.* in 1983[3]. Compared with single-wavelength lasers, polychromatic light has broad spectrum; thus, it has been applied to the treatment of various diseases, including skin vascular, skin pigment, hirsutism, skin aging, and photoaging. In fact, photoaged skin treatment is the main application of polychromatic lights. Thus, the greatest benefit of IPL photorejuvenation is that it can treat a wide range of skin problems. With IPL therapy, patients undergo a single type of treatment for multiple skin conditions, rather than having to undergo several procedures with laser therapy. However, most of the current works focus on single-wavelength lasers[4−6]. Although several works on the clinical applications and efficacies of IPL[7−11] exist, most of these publications concern the thermal-effect measurement and simulation of the biological tissues irradiated by the polychromatic light. Meanwhile, the existing simulation methods are mostly built on the assumption that the IPL spectrum energy output is uniform. In this letter, we put forward a method to measure the spectral-energy distribution of the polychromatic light. Based on the fact that the thermal effect of single-wavelength light irradiating biological tissue can be calculated, and the thermal effects produced by different wavelengths satisfy the superposition principle, the thermal effect of the polychromatic. light can be calculated. We propose a new strategy based on finite element method (FEM) to overcome the above shortcomings of the current work on IPL to some extent.

The most widely used bioheat transfer equation is the classic Pennes equation, which fundamentally distinguishes the heat-transfer problems between biological tissues and general engineering materials for the first time[12]. Based on this equation, the more detailed calculation of the temperature distribution and the analysis of the heat transfer in bio-tissue are available. The Pennes equation is formulated as follows[12]

$$\rho C\frac{\partial T}{\partial t} = k\nabla^2 T + Q_{\rm b} + Q_{\rm m} + Q_{\rm r}, \tag{1}$$

where ρ is the tissue density (kg/m^3); C is the tissue specific heat (J/(kg·K)); T is the tissue temperature (°C); k is the tissue thermal conductivity (W/(m·K)); $Q_{\rm b} = W_{\rm b}C_{\rm b}\cdot(T_{\rm b} - T)$ is the heat due to blood flow (i.e., the heat change caused by the blood perfusion); $W_{\rm b}$ is the blood-perfusion rate (kg·/(s·m^3)); $C_{\rm b}$ is the blood specific heat (J·/(kg· K)); T_b is the blood temperature (°C); $Q_{\rm m}$ is the metabolic heat generation per unit volume (W/(m)^3); and $Q_{\rm r}$ is the external heat generation per unit volume (W/(m)^3).

In Eq. (1), the blood-flow and metabolism components could be ignored in the experimental study of *in vitro* biological tissue. In the case when *in vitro* biological tissue is considered, Eq. (1) can be simplified as

$$\rho C\frac{\partial T}{\partial t} = k\nabla^2 T + S. \tag{2}$$

If the axisymmetric Gaussian distribution laser beam is used, the heat component S can be expressed as[13−15]

$$S = \mu_{\rm a}(1-R)\phi_0 \times \exp[-0.5\frac{r^2}{w_0^2}\exp(-\mu_{\rm s}z) - \mu_{\rm t}z]\exp[-4(t-\tau)^2/\tau^2]. \quad (3)$$

If the axisymmetric uniform distribution circular flat beam is applied, the heat component can be expressed as[15]

$$S = \mu_{\rm a}(1-R)\phi_0 {\rm Round}\left[0.3647+\exp(-2r/w_0)\right] \times \exp(-\mu_{\rm t}z){\rm Round}\left[0.1321+\exp(-t/\tau)\right], \quad (4)$$

where μ_α ($\rm cm^{-1}$) is the tissue-absorption coefficient; $\mu_{\rm s}$ ($\rm cm^{-1}$) is the tissue-scattering coefficient; $\mu_{\rm t} = \mu_\alpha + \mu_{\rm s}$ is the tissue-attenuation coefficient; $\phi_0 = 2P/(\pi w_0^2)$ ($\rm W/cm^2$) is the incident-light flux density, w_0 (cm) is the radius of the beam of incident light (or the waist of the Gaussian beam); R is the specular reflectivity; t(s) is the computation time; τ(s) is the function time for the light source (for the pulsed light, τ is the pulse duration). Round (number, digits) is the round function which returns a number rounded to a specified number of digits (e.g., Round (0.47, 1)=0.5, Round (0.54, 0)=1). If the digit is omitted, then the round function will return an integer. When $t > \tau$ or $r > w_0$, the heat source component is zero.

If the broad-spectrum polychromatic light is considered, the heat-source component $S_{\rm all}$ should include various absorbed heat components of all kinds of wavelengths in the entire spectral range of the light source. Therefore, we propose that the heat-source item of the axisymmetric Gaussian distribution polychromatic light should be formulated as

$$S_{\rm all} = \sum_i \mu_{\rm a}(i)[1-R(i)]\phi_0 w_i \times\exp\{-0.5\frac{r^2}{w_0^2}\exp[-\mu_{\rm s}(i)z] - \mu_{\rm t}(i)z\}\exp[-4(t-\tau)^2/\tau^2]. \quad (5)$$

Accordingly, the expression of axisymmetric uniform distribution circular polychromatic light is

$$S_{\rm all} = \sum_i \mu_{\rm a}(i)[1-R(i)]\phi_0 w_{\rm i}{\rm Round}[0.3647+\exp(-2r/w)] \times\exp(-\mu_{\rm t}(i)z){\rm Round}[0.1321+\exp(-t/\tau)], \quad (6)$$

where $\mu_\alpha(i)$, $\mu_{\rm s}(i)$, $\mu_{\rm t}(i)$, and $R(i)$ are the absorption coefficient, scattering coefficient, attenuation coefficient, and specular reflectivity parameters, respectively, at the wavelength of i. The new parameter $w_{\rm i}$ is the corresponding spectrum ratio for the wavelength, also known as weights, which satisfies

$$\sum_{i=1}^{\rm all} w_i = 1. \quad (7)$$

To conduct modeling or numerical simulation of the polychromatic light, we need to solve the following two key problems:

1) the spectrum distribution of the polychromatic light source;

2) the optical properties of the tissue under different wavelengths or frequencies, including the absorption and scattering coefficients.

In order to validate the theoretical calculation of the computational model of polychromatic light, we use a continuous xenon lamp as the light source and use commercially available fresh porcine skin and *in vitro* liver tissue as samples in the experiments. The thermal and optical parameters used in the simulation are as follows[15−18]: for porcine skin, $\rho = 1.075$ g/cm^3, $C = 3.5$ J/(g·°C), and $k = 4.5$ mW/(cm·K), whereas for the liver, $\rho = 1.09$ g/cm^3, $C = 3.35$ J/(g·K), and $k = 4.2$ mW/(cm· K). The optical parameters of the porcine skin and liver are as follows: for porcine skin tissue, $n = 1.37$ and $g = 0.85$, whereas for the liver tissue, $n = 1.37$ and $g = 0.92$. The absorption coefficient $\mu_{\rm a}$ and scattering coefficient $\mu_{\rm s}$ of the porcine skin tissue in different wavelengths (400–810 nm, in steps of 10 nm) used in the simulation were taken from Ref. [19], where smooth surfaces were assumed. The absorption coefficient $\mu_{\rm a}$ and scattering coefficient $\mu_{\rm s}$ of the porcine liver tissue over different wavelengths were obtained from Ref. [20], where native porcine liver was assumed.

The spectrum distribution measurement was divided in two steps.

1) Various narrow bandwidth light sources with different wavelengths were employed to measure the transmission efficiency of the monochromator at different wavelengths: the lasers, characteristic wavelengths of the mercury lamp, and light-emitting diodes, whose bandwidth was less than that of the monochromator.

2) The foregoing monochromator was used to measure the power-spectrum distribution of the xenon lamp. An optical power meter (SJG-100 mV, Shanghai Instrument Co.) was used to measure each single wavelength as well as energy calibration.

After steps 1) and 2), the actual power spectrum of the xenon lamp was obtained.

Figure 1 shows the curve of the spectrum distribution of the aforementioned xenon lamp through filters. These filters are used to limit the spectrum in the wavelength range of interest.

The settings of the experiments are as follows. The light source is a continuous xenon lamp (L2274, Hamamatsu, Japan). Through the post filters, the wavelength range is limited in the range of 400–810 nm. The lens

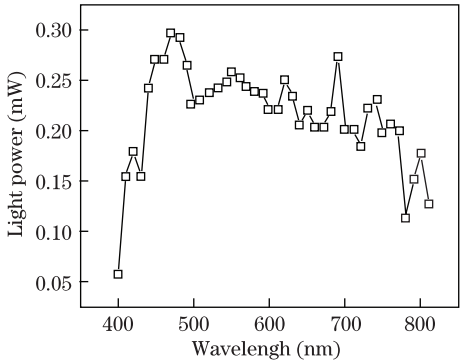

Fig. 1. Power distribution of continuous xenon lamp though filters.

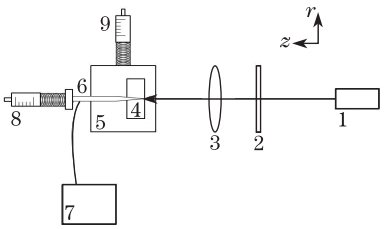

Fig. 2. Scheme of the experimental setup. (1: Xenon lamp, 2: filters, 3: focusing lens, 4: sample box, 5: two-dimensional spiral micrometer platform, 6: K-type thermocouple probe needle, 7: TES-1310 digital thermometer, and 8 and 9: screw micrometers).

focuses the light radiation on the tissue vertically in a radius of approximately 1.5 mm. The thermometer device is digital thermometer (TES-1310, Taiwan taike Shi, Taiwan) with temperature range from –50.0 to 199.9 °C. The experimental optical path diagram is shown in Fig. 2. Two screw micrometers, 8 and 9, can change the position of the tissue in two directions. Screw micrometer 8 and the K-type thermocouple temperature probe is connected to move the probe position in the axial direction and to detect the temperature of the surface of the tissue, as well as the different depths within it. Using screw micrometer 9, the tissue can be moved in the radial direction. The sample box is a square wooden structure with a plane glass; thus, the heat absorption in its three surfaces can be ignored. The light is incident on tissues through the glass. The transmittance of the glass is also considered during simulation.

For the sample, firstly, we cut the tissue into the same size as the foregoing sample box. Secondly, we kept the surface of the tissue wet with physiological saline to maintain its activity and moisture. Thirdly, we set aside the sample in the laboratory until the temperature of the sample equaled room temperature, after which we placed the tissue in the sample box for testing. Porcine skin and liver were selected as sample according to available biotissue optical and thermal parameters in different wavelengths reported. The tissue temperatures at the surface position (0 mm, 0 mm) and inner position (0 mm, 0.5 mm) were then measured.

FEM are widely used in analyzing and dealing with heat conduction and distribution in biological issues. In FEM, the basic idea is to divide the object into a finite number of units (including a number of nodes). The heat-balance equation in each node under certain boundary and initial conditions with consideration to the law of conservation of energy can then be solved. We can also calculate the temperature of each node and cell and other related quantities. Generally speaking, the smaller the element is divided, the more accurate the calculated result would be. However, if the elements are too small, the computational time will be too long. Thus, to consider the specificity of the biological tissue as well as the demand for accuracy, the infinite element mesh is divided into the size of cells (approximately tens of microns). Furthermore, for simplicity, single-layer axial symmetry is chosen as the structure model. The cortical thickness is 2 cm. Adiabatic boundary is imposed to the symmetrical axis, and natural convection boundary condition is imposed to the surface of the skin. The convection coefficient is 6.2×10^{-4} W/(cm· K). The uniform distribution of the circular flat beam heat-entry form is used as the heat-source component. FEM and the aforementioned heat-source form of broad-spectrum light source are used to compute the temperature response of the porcine skin and liver under continuous-output xenon lamp.

Because listing the incident light power of every wavelength would be impossible and only part of the wavelength of the optical and thermal parameters of the biological tissue has been reported, we simulate the process by using approximate and simplified means as follows:

Step 1. Calculate the power of the incident light from 400 to 810 nm with an interval of 10 nm;

Step 2. Obtain the optical and thermal parameters of the biological tissues from published papers from 400 nm with an interval of 10 nm;

Step 3. Assume that 10 nm is such a small wavelength range. The parameters obtained from steps 1 and 2 are used to represent each wavelength parameter within the corresponding 10-nm scope;

Step 4. Apply FEM method to simulate the optothermal process for every 10 nm and calculate the resulting temperature rise for every 10 nm;

Step 5. Calculate the sum of each resulting temperature rise for every 10 nm, and obtain the overall temperature rise for the whole scope of wavelength.

The porcine skin temperatures on the surface position (0 mm, 0 mm) and at the inner position (0 mm, 0.5 mm) were measured and calculated. The comparison chart of the experimental and simulation results is shown in Fig. 3.

Figure 3 shows that the temperature curve due to tissue depth is divided into two groups. The one with higher temperature rise is the porcine-skin temperature on the surface (0 mm, 0 mm), whereas the lower temperature rise is the temperature at the inner position (0 mm, 0.5 mm) on the axial direction. On the surface of the porcine skin, after 120-s irradiation by the light source, the increase in the temperature given by our experiment is approximately 1.9 °C, whereas the FEM simulation result is 1.6 °C. Considering the temperature at the position (0 mm, 0.5 mm) in this tissue, after 120-s irradiation, the increase in the temperature is 1.2 °C, whereas that in the simulation result is 1.1 °C. The results show that the experiment and simulation match each other quite well.

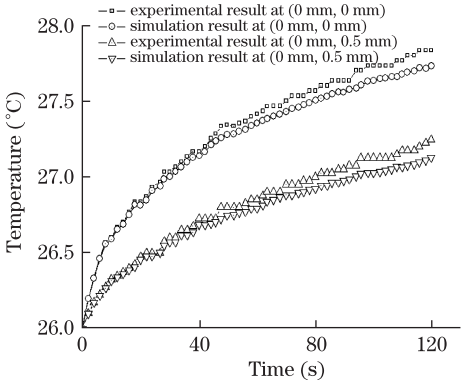

Fig. 3. Temperature versus irradiation time curve of the experimental and simulation results of porcine skin.

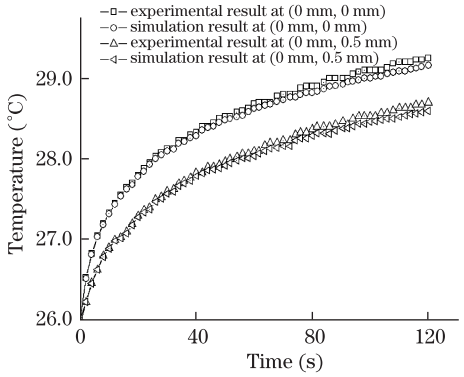

Fig. 4. Temperature versus irradiation time curve of the experimental and simulation results of porcine liver.

In order to validate the general applicability of the method, we use the same light source to perform same experiment on porcine liver and use the same FEM program to simulate. The porcine liver temperatures at the surface position (0 mm, 0 mm) and the inner position (0 mm, 0.5 mm) are measured and calculated also. Figure 4 shows that, due to the relative higher moisture content of the porcine liver (compared with the porcine skin), the temperature increase of the porcine liver is more evident. Because of different depth of the measurement and simulation, the curves in Fig. 4 also can be divided into two groups. In the first group, a relative higher temperature increase on the surface of the porcine liver sample is evident at the incident point of light (0 mm, 0 mm), whereas, in the second group, the temperature curve at point (0 mm, 0.5 mm) is along the axial direction. On the surface of the porcine liver at point (0 mm, 0 mm), after 120-s irradiation by the light source, the increase in temperature given by our experiment is approximately 3.3 °C, whereas the FEM simulation result is 3.1 °C. The increase in temperature at the depth of (0 mm, 0.5 mm) in this sample after 120-s irradiation is 2.7 °C, whereas the simulation result is 2.6 °C. The difference is smaller than the results obtained from the porcine skin tissue.

Although the foregoing elementary result is an approximation, it is still meaningful. We have proposed a method for solving the problem of optical-temperature response of biological tissue under polychromatic light and have provided the superposition relationship of optical-thermal effects in different wavelengths for the first time.

In conclusion, because of broader spectrum and various symptom adaptabilities, polychromatic light is favored and has a good prospect in the photorejuvenation and beauty realms. It has also become a popular topic of study. In this letter, a FEM computation model for analyzing optothermal interaction of polychromatic light and biology tissue is proposed. Through the FEM, we simulate the temperature distribution in the porcine skin and liver, and perform the experimental measurement. The results of both simulation and experiment are commendably matched.

This work was supported by the National Natural Science Foundation of China (No. 60678054) and the Key Laboratory of Optoelectronic Science and Technology for Medicine (Fujian Normal University), Ministry of Education, China.

References

1. P. H. Bitter Jr., Dermatol. Surg. **26,** 835 (2000).
2. K. Gu, Q. Ren, and W. Li, Acta Laser Biology Sin. (in Chinese) **29,** 205 (2001).
3. R. R. Anderson and J. A. Parrish, Science **220,** 524 (1983).
4. H. Ding, M. Huang, Y. Tong, Z. Li, S. Xie, and W. Gong, Acta Opt. Sin. (in Chinese) **28,** 1983 (2008).
5. J. J. Crochet, S. C. Gnyawali, Y. Chen, E. C. Lemley, L. V. Wang, and W. R. Chen, J. Biomed. Opt. **11,** 034031 (2006).
6. W. Gong, Y. Huang, and S. Xie, Chin. Opt. Lett. **7,** 512 (2009).
7. D. J. Goldberg and J. Samady, Laser. Surg. Med. **28,** 141 (2001).
8. D. J. Goldberg and K. B. Cutler, Laser. Surg. Med. **26,** 196 (2000).
9. C. Raulin, B. Greve, and H. Grema, Laser. Surg. Med. **32,** 78 (2003).
10. J. Myhill, W. B. Umler, L. Hennings, E. D. Bearden, L. M. Buckmiller, and G. Shafirstein, Medical Laser Appl. **23,** 71 (2008).
11. K. Negishi, Y. Tezuka, N. Kushikata, and S. Wakamatsu, Dermatol. Surg. **27,** 627 (2001).
12. H. H. Pennes, J. Appl. Physiol. **1,** 93 (1948).
13. A. Welch, IEEE J. Quantum Electron. **20,** 1471 (1984).
14. A. L. McKenzie, Phys. Med. Biol. **28,** 905 (1983).
15. X. Li, "Numerical analysis and experimental research on laser induced thermal effect in bio-tissues" PhD. Thesis (Tianjin University, 2004).
16. T. L. Troy and S. N. Thennadil, J. Biomed. Opt. **6,** 167 (2001).
17. C. R. Simpson, M. Kohl, M. Essenpreis, and M. Cope, Phys. Med. Biol. **43,** 2465 (1998).
18. R. Groenhuis, H. A. Ferwerda, and J. Bosch, Appl. Opt. **22,** 2456 (1983).
19. X. Ma, J. Q. Lu, H. Ding, and X. H. Hu, Opt. Lett. **30,** 412 (2005).
20. J. P. Ritz, A. Roggan, C. Isbert, G. Müller, H. J. Buhr, and C. T. Germer, Laser. Surg. Med. **29,** 205 (2001).